Super-elastic collisions of thermal activated nanoclusters

Hisao Hayakawa[†],   Hiroto Kuninaka[§]

[†]hisao@yukawa.kyoto-u.ac.jp,[§]kuninaka@phys.chuo-u.ac.jp

Abstract

Impact processes of nanoclusters subject to thermal fluctuations are investigated, theoretically. In the former half of the paper, we discuss the basis of quasi-static theory. In the latter part, we carry out the molecular dynamics simulation of collisions between two identical nanoclusters, and report some statistical properties of impacts of nanoclusters.

1 Introduction

The initial kinetic energy of colliding bodies is distributed into the internal degrees of freedom in an inelastic collision. Such a collision is characterized by the restitution coefficient $e \equiv V'/V$, where V and V' are, respectively, the relative colliding speed and the relative rebound speed. Although it is believed that the restitution coefficient e satisfies $e < 1$ for impacts of macroscopic bodies, the anomalous impact with $e > 1$ is possible in some special situations for small bodies. Indeed, the prohibition of $e > 1$ is originated from the second law of thermodynamics[1, 2], but some terms which disappear in the thermodynamic limit play important roles in the description of small systems. It should be noted that the restitution coefficient projected into the normal direction of the collision can easily exceed unity in the case of oblique collisions.[3, 4]

The low-speed collisions for macroscopic bodies are believed to be described by the quasi-static theory, which is consistent with some experimental results.[5, 6, 7] However, it is not obvious whether the quasi-static theory is applicable to the impact of nanoclusters. Indeed, we expect that the effects of cohesive force among atoms cannot be ignored for such small systems. Awasthi *et al.*[8] reported that the dependence of the restitution coefficient e on the impact speed for nanoclusters, which contain adhesions, differs from the prediction from the quasi-static theory based on their molecular dynamics simulation (MDS). In a recent paper, Brilliantov *et al.* extend the quasi-static theory to the theory of cohesive collisions.[9]

The physics of nanoclusters is one of hot subjects. The MDS is a standard tool to investigate collisions of nanoclusters such as fulleren. Some of such studies focus on fragmentations and coalescences after binary collisions of nanoclusters[10, 11, 12]. The other studies discuss the collisions of a cluster with a substrate[8], the erosion

process on a diamond surface[13], and the fragmentation pattern of clusters[14]. So far, we do not know any paper to investigate the effects of thermal fluctuations on collisions of nanoclusters except for our preliminary report.[15]

In this paper, we perform the MDS of colliding clusters to investigate the effect of thermal fluctuations. This is the extension of our previous work.[15] In the first part, we review what model is adequate to describe the collision of nanoclusters. In the next section, we introduce the generalized Langevin equation and the fluctuation-dissipation relation in the first kind. In section 3, we calculate the velocity autocorrelation function (VACF) of a lattice model to apply it to a system of a nanocluster. Then, we justify the quasi-static theory to describe the collisions of nanoclusters. In the second part, we show the detailed results of our numerical simulations. In section 4, we introduce our numerical model of the MDS. In section 5, we explain the results of our simulation, which consist of four subsections. In the first subsection, we check the relaxation of VACF in our model. In the next subsection, we demonstrate sequential snapshots of collisions between two identical nanoclusters. In section 5.3, we compare our numerical result of the impact speed dependence of the restitution coefficient with the quasi-static theory of cohesive or noncohesive collisions. In section 5.4, we show the frequency distribution functions of the restitution coefficient and their dependence on cohesive force between atoms. We also show the probabilities to appear four categories in our simulation when the cohesive parameter is finite. In section 6, we discuss and summarize our results.

2   The Langevin equation

It is well known that we can formally rewrite the Newtonian equation of motion as the generalized Langevin equation for the 'slow' variable. When we consider the motion of colliding a pair of small clusters, it is natural to adopt the relative velocity $\boldsymbol{v}$ between the center of mass of each cluster as the 'slow' variable[16]. We should note that the center of mass is characterized by the total mass of one cluster, while each element of the cluster can be characterized by the mass for the element. Thus, the effective mass of the center of mass is much larger than the mass of the element. Thus, the generalized Langevin equation is given by

$$\frac{d\boldsymbol{v}}{dt} = -\int_{-\infty}^{t} dt' \gamma(t-t')\boldsymbol{v}(t') + \boldsymbol{\theta}(t) + \frac{\boldsymbol{F}(t)}{M}, \tag{1}$$

where $\gamma(t)$, $\boldsymbol{\theta}(t)$, M, and $\boldsymbol{F}(t)$ are the memory kernel, the fluctuating force from the fast oscillations, the reduced mass of two clusters, and the systematic force acting on the centers of mass, respectively. The fluctuation force $\boldsymbol{\theta}(t)$ is believed to be unimportant for the impact problem of two clusters. The systematic force $\boldsymbol{F}(t)$ may be approximated by the Hertzian contact force. From the fluctuation-dissipation relation in the first kind, the Laplace transform $\hat{\gamma}(\omega) \equiv \int_0^\infty dt\gamma(t)e^{-i\omega t}$ satisfies

$$(i\omega + \hat{\gamma}(\omega))^{-1} = \frac{M}{T} \int_{-\infty}^{\infty} dt\langle \boldsymbol{v}(0) \cdot \boldsymbol{v}(t)\rangle e^{-i\omega t}, \tag{2}$$

where T is the temperature, and the Boltzmann constant is set to be unity[17]. We should note that $\hat{\gamma}(\omega)$ can be defined as the usual Fourier transform if we assume

$\gamma(t) = \gamma(-t)$ for $t < 0$. If the integration of the velocity autocorrelation function (VACF), *i.e.* $\int_0^\infty dt \langle \boldsymbol{v}(0) \cdot \boldsymbol{v}(t) \rangle$ is finite, $\hat{\gamma}(\omega \to 0)$ is finite. In this case, the generalized Langevin equation can be approximated by the Langevin equation with the white noise satisfying $\langle \theta_i(t) \cdot \theta_j(t') \rangle = 2T\gamma \delta_{i,j} \delta(t - t')$ where $\theta_i(t)$ is the i-th component of $\boldsymbol{\theta}(t)$. It is obvious that this Langevin equation is an irreversible equation. Thus, the behavior of VACF is the most important to characterize the macroscopic dissipation.

3 The relaxation of the correlation function

As discussed in the previous section, the relaxation of VACF plays a key role for the equilibration process of a system. Let us consider the relaxation of VACF in a nanocluster which consists of a regular lattice with equal-mass atoms. When the atoms are confined in attractive potential, the excitation from the ground state is characterized by the harmonic oscillation in a simple cubic lattice. In this section, we demonstrate that VACF of a uniform system in the simple cubic lattice exhibits the slow relaxation proportional to $1/\sqrt{t}$. The analysis presented here is the straightforward extension of the one-dimensional cases.[16]

Let us consider an infinitely large simple cubic lattice system in which the mass points with mass m connecting with the linear spring whose spring constant is k. The position of each lattice point can be specified by a set of integer $\boldsymbol{n} = (n_x, n_y, n_z)$ in this system. Introducing the characteristic angular frequency $\omega_0 \equiv \sqrt{k/m}$, the equation of motion of the deviation from the equilibrium position $\boldsymbol{r_n}(t)$ obeys

$$\ddot{\boldsymbol{r}}_{\boldsymbol{n}}(t) = -\omega_0^2 \left(6\boldsymbol{r}_{\boldsymbol{n}}(t) - \sum_{i=1}^{6} \boldsymbol{r}_{\boldsymbol{n}+\hat{\boldsymbol{e}}_i}(t) \right), \tag{3}$$

where $\hat{\boldsymbol{e}}_1 = (1,0,0)$, $\hat{\boldsymbol{e}}_2 = (-1,0,0)$, $\hat{\boldsymbol{e}}_3 = (0,1,0)$, $\hat{\boldsymbol{e}}_4 = (0,-1,0)$, $\hat{\boldsymbol{e}}_5 = (0,0,1)$ and $\hat{\boldsymbol{e}}_6 = (0,0,-1)$.

Let us introduce the lattice Fourier transform and the inverse Fourier transform as

$$\hat{\boldsymbol{r}}_{\boldsymbol{k}}(t) \equiv \sum_{\boldsymbol{n}} e^{-i\boldsymbol{k}\cdot\boldsymbol{n}} \boldsymbol{r}_{\boldsymbol{n}}(t), \quad \boldsymbol{r}_{\boldsymbol{n}}(t) = \frac{1}{(2\pi)^3} \int d\boldsymbol{k} e^{i\boldsymbol{k}\cdot\boldsymbol{n}} \hat{\boldsymbol{r}}_{\boldsymbol{k}}(t), \tag{4}$$

where $\sum_{\boldsymbol{n}} = \sum_{n_x=-\infty}^{\infty} \sum_{n_y=-\infty}^{\infty} \sum_{n_z=-\infty}^{\infty}$ and $\int d\boldsymbol{k} = \int_{-\pi}^{\pi} dk_x \int_{-\pi}^{\pi} dk_y \int_{-\pi}^{\pi}$. Thus, the equation of motion in the Fourier space is given by

$$\ddot{\hat{\boldsymbol{r}}}_{\boldsymbol{n}}(t) = -4\omega_0^2 \sum_{i=1}^{3} \sin^2 \left(\frac{k_i}{2} \right) \hat{\boldsymbol{r}}(t). \tag{5}$$

Furthermore, introducing the Laplace transform $\tilde{\boldsymbol{r}}_{\boldsymbol{k}}(z) \equiv \int_0^\infty dt e^{-zt} \hat{\boldsymbol{r}}_{\boldsymbol{k}}(t)$, we obtain

$$\tilde{\boldsymbol{r}}_{\boldsymbol{k}}(z) = \frac{z\hat{\boldsymbol{r}}_{\boldsymbol{k}}(0) + \dot{\hat{\boldsymbol{r}}}_{\boldsymbol{k}}(0)}{z^2 + 4\omega_0^2 \sum_{i=1}^{3} \sin^2 \left(\frac{k_i}{2} \right)}. \tag{6}$$

Let us consider the motion of the mass point at the center of the mass in the system. From the relation $\boldsymbol{r_0}(t) = \int \frac{d\boldsymbol{k}}{(2\pi)^3} \hat{\boldsymbol{r}}_{\boldsymbol{k}}(t)$, we reach

$$\bar{\boldsymbol{r}}_{\boldsymbol{0}}(z) = \frac{1}{(2\pi)^3} \int d\boldsymbol{k} \frac{z\hat{\boldsymbol{r}}_{\boldsymbol{k}}(0) + \dot{\hat{\boldsymbol{r}}}_{\boldsymbol{k}}(0)}{z^2 + 4\omega_0^2 \sum_{i=1}^{3} \sin^2 \left(\frac{k_i}{2} \right)}. \tag{7}$$

where we have used $\bar{\boldsymbol{r}}_{\boldsymbol{n}}(z) \equiv \int_0^\infty dt e^{-zt} \boldsymbol{r}_{\boldsymbol{n}}(t)$.

Here, VACF at the center of the mass is defined by

$$\phi(t) \equiv \langle \dot{\boldsymbol{r}}_{\boldsymbol{0}}(0) \cdot \dot{\boldsymbol{r}}_{\boldsymbol{0}}(t) \rangle, \tag{8}$$

where $\langle \cdots \rangle$ represents the ensemble average over the different initial conditions. We assume that the initial condition satisfies

$$\langle \dot{\boldsymbol{r}}_{\boldsymbol{m}}(0) \cdot \dot{\boldsymbol{r}}_{\boldsymbol{n}}(0) \rangle = \phi(0)\delta_{\boldsymbol{m,n}} = \frac{3T}{m}\delta_{\boldsymbol{m,n}}, \quad \langle \boldsymbol{r}_{\boldsymbol{n}}(0) \cdot \dot{\boldsymbol{r}}_{\boldsymbol{0}}(0) \rangle = 0. \tag{9}$$

Then, the Laplace transform $\tilde{\phi}(z) \equiv \int_0^\infty e^{-zt}\phi(t) = z\langle \bar{\boldsymbol{r}}_{\boldsymbol{0}}(z) \cdot \dot{\boldsymbol{r}}_{\boldsymbol{0}}(0) \rangle$ of $\phi(t)$ satisfies

$$\begin{aligned}
\tilde{\phi}(z) &= \frac{1}{(2\pi)^3} \frac{z\langle \hat{\boldsymbol{r}}_{\boldsymbol{k}}(0) \cdot \dot{\boldsymbol{r}}_{\boldsymbol{0}}(0) \rangle + \langle \dot{\hat{\boldsymbol{r}}}_{\boldsymbol{k}}(0) \cdot \dot{\boldsymbol{r}}_{\boldsymbol{0}}(0) \rangle}{z^2 + 4\omega_0^2 \sum_{i=1}^3 \sin^2\left(\frac{k_i}{2}\right)} \\
&= \frac{3Tz}{(2\pi)^3 m} \int d\boldsymbol{k} \frac{1}{z^2 + 4\omega_0^2 \sum_{i=1}^3 \sin^2\left(\frac{k_i}{2}\right)}, \tag{10}
\end{aligned}$$

where we have used $\langle \dot{\hat{\boldsymbol{r}}}_{\boldsymbol{k}}(0) \cdot \dot{\boldsymbol{r}}_{\boldsymbol{0}}(0) \rangle = 3T/m$. From the inverse Laplace transform of $\tilde{\phi}(z)$ we obtain the expression

$$\phi(t) = \frac{3T}{m} \int \frac{d\boldsymbol{k}}{(2\pi)^3} \cos\left[2\omega_0 t \sqrt{\sum_{i=1}^3 \sin^2\left(\frac{k_i}{2}\right)}\right]. \tag{11}$$

Since the direct integration of (11) is difficult and we are not interested in the detailed properties of the lattice, we may introduce the approximation $\sum_{i=1}^3 \sin^2 \frac{k_i}{2} \simeq \sum_{i=1}^3 k_i^2/4 = k^2/4 \simeq \sin^2 \frac{k}{2}$, where $k \equiv \sqrt{\sum_{i=1}^3 k_i^2}$. Once we adopt such an approximation, we obtain

$$\phi(t) \simeq \frac{3T}{2\pi^2 m} \int_0^\pi dk k^2 \cos\left[2\omega_0 t \sin\frac{k}{2}\right] \tag{12}$$

From the numerical integration of this expression, it is clearly to find $\phi(t) \sim 1/\sqrt{t}$ (see Fig. 1). Indeed, when we put $\tau \equiv 2\omega_0 t \sin k/2$, there is the relation $k^2 dk = 4dk - 4d\tau/(\omega_0 t) + O(k^4 dk)$. If we ignore the terms of $k^4 dk$, we obtain the approximate relation $I(t) \equiv \int_0^\pi dk k^2 \cos[2\omega_0 t \sin k/2] \simeq 4\pi J_0(2\omega_0 t) - 4\sin(2\omega_0 t)/(\omega_0 t)$. From the asymptotic form of the Bessel function, we obtain $I(t) \simeq \sqrt{\pi/(\omega_0 t)}\cos(2\omega_0 t - \pi/4)$ for $\omega_0 t \gg 1$. This result is essentially the same as that for one-dimensional case $\phi(t) \propto J_0(2\omega_0 t)$. This time dependence of VACF can be observed in the direct simulation of nanoclusters in which each cluster is a 13 layer of the spherical cut of face-centered cubic (FCC) lattice , i.e. 682 Lennard-Jones atoms (Fig.3). The setup of our simulation will be explained in the latter part.

In spite of this extremely slow relaxation under the absence of $\hat{\gamma}(0)$, we can approximately define the friction constant in the Langevin equation to describe the low frequency behaviors. Actually, if we adopt the approximation $\phi(t) \simeq \alpha\cos(\omega_0 t)/\sqrt{\omega_0|t|}$ with a constant α for large t, substituting this into (2) we obtain

$$(i\omega + \hat{\gamma}(\omega))^{-1} = \alpha\frac{m}{T}\left\{\frac{1}{\sqrt{|2\omega_0 - \omega|}} + \frac{1}{\sqrt{2\omega_0 + \omega}}\right\} \simeq \frac{\sqrt{2}\alpha m}{T\sqrt{\omega_0}}\left(1 + \frac{1}{4}\left(\frac{\omega}{2\omega_0}\right)^2 + \cdots\right) \tag{13}$$
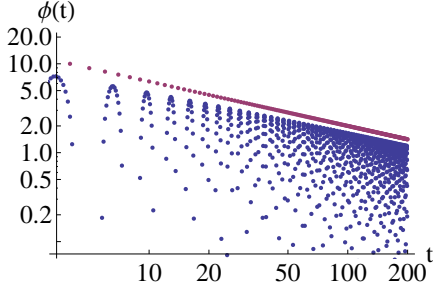
Figure 1: A log-log plot of the decay of VACF. Here the time is normalized by ω_0 and the guide line represents $20/\sqrt{t}$.
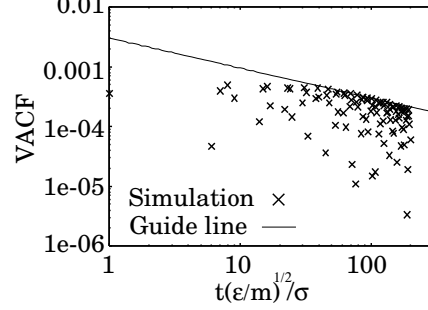

Figure 2: The comparison between VACF of the center of mass of the upper cluster (cross points) and fitting line proportional to $1/\sqrt{t}$, where the time is dimensionless time for the MDS.

for $\omega \ll \omega_0$. Thus, we may approximate $\gamma(t) = \int_{-\infty}^{\infty} d\omega/2\pi e^{i\omega t}\hat{\gamma}(\omega)$ by

$$\gamma(t) \simeq \Omega\delta(t) - \frac{d\delta(t)}{dt} \tag{14}$$

where $\delta(t)$ is Dirac's delta function and $\Omega \equiv T\sqrt{\omega_0}/(\sqrt{2}\alpha m)$. Thus, the memory term can be approximated by

$$\int_{-\infty}^{t} dt'\gamma(t')\boldsymbol{v}(t') \simeq \Omega\boldsymbol{v}(t) + \frac{d\boldsymbol{v}}{dt} - \delta(0)\boldsymbol{v}(t), \tag{15}$$

where the last term can be absorbed in the initial condition. Finally, we obtain the effective Langevin equation for the low frequency behavior at $t \neq 0$ as

$$\frac{d\boldsymbol{v}}{dt} = -\frac{\Omega}{2}\boldsymbol{v} + \frac{\boldsymbol{\theta}}{2} + \frac{\boldsymbol{F}}{2M} \tag{16}$$

which does not have any essential difference from the conventional Langevin equation. This may justify to use the quasi-static theory even when we consider a collision between nanoclusters of a uniform lattice system. Indeed, once we accept to use the Langevin equation, it is straightforward to derive the quasi-static theory of macroscopic collisions.[5, 6, 7]

It should be noted that the motion of the atom at the center of mass can be described by the equation of motion for a harmonic oscillator. In order to use eq.(1), we need to introduce some tricks, such as the mass difference, the contact with the other atoms and the nonlinearity. However, this argument may be instructive to understand the basis of the Langevin equation from the mechanical point of view.

4   Our numerical model

Let us introduce our numerical model. Our model consists of two identical clusters. Each of them is the spherical cut from a 13 layered face-centered cubic (FCC) lattice

5

and consisted of 682 "atoms". When we simulate larger size of nanoclusters, the system is fluidized in the vicinity of surface, while the data for the smaller systems strongly depend on the specific orientation of impacts. The details of system size dependence of the simulation will be reported elsewhere.

The clusters have facets because of the small number of "atoms" (Fig. 3). All the "atoms" in each cluster are bounded by the Lennard-Jones potential $U(r_{ij})$ as

$$U(r_{ij}) = 4\epsilon \left\{ \left(\frac{\sigma}{r_{ij}} \right)^{12} - a \left(\frac{\sigma}{r_{ij}} \right)^{6} \right\}, \tag{17}$$

where r_{ij} is the distance between two "atoms", i and j. The coupling coefficient of the attractive term a is treated as a cohesive parameter between atoms on the surfaces of one cluster and those on the surface of another, while the potential act on the atoms within the same cluster satisfies $a = 1.0$. Here, we will consider collisions for the control parameters $a = 0$ and $a = 0.2$ between different clusters.[8]. In eq.(17), ϵ is the energy constant and σ is the lattice constant. When we regard the "atom" as argon, the values of the constants become $\epsilon = 1.65 \times 10^{-21}$J and $\sigma = 3.4$Å, respectively. [18] Henceforth, we label the upper and the lower clusters as cluster C^u and cluster C^l, respectively. To reduce computational costs, we introduce the cut-off length σ_c of the Lennard-Jones interaction as $\sigma_c = 2.5\sigma$.

The procedure of our simulation is as follows. The initial velocities of the "atoms" in both C^u and C^l satisfy the Maxwell-Boltzmann distribution at the initial temperature T. The initial temperature is set to be $T = 0.01\epsilon$ or $T = 0.02\epsilon$ in most of our simulations. Sample average is taken over different sets of initial velocities governed by the Maxwell-Boltzmann velocity distribution for "atoms".

To equilibrate the clusters, we adopt the velocity scaling method [19, 20] for 2000 steps in the initial stage of simulations. We have checked the equilibration of the total energy in the initial relaxation process. After the equilibration, we give translational velocities to C^u and C^l at the relative separation σ_c between two clusters to make them collide against each other, where the initial colliding speed is achieved by the acceleration $g = 0.01\epsilon/(m\sigma)$ from a stationary state. The relative speed of impact ranges from $V = 0.02\sqrt{\epsilon/m}$ to $V = 0.07\sqrt{\epsilon/m}$, which are less than the thermal velocity for one "atom" defined by $\sqrt{T/m}$, where m is the mass of the "atom".

Numerical integration of the equation of motion for each atom is carried out by the second order symplectic integrator with the time step $dt = 1.0 \times 10^{-2}\sigma/\sqrt{\epsilon/m}$. The rate of energy conservation, $|E(t) - E_0|/|E_0|$, is kept within 10^{-5}, where E_0 is the initial energy of the system and $E(t)$ is the energy at time t.

We let the angle around $z-$axis, θ^z, be $\theta^z = 0$ when the two clusters are located in mirror-symmetric positions with respect to $z = 0$. In most of our simulation, we adopt the data at $\theta^z = 0$. From our impact simulation for $\theta_i^z = \pi i/18$ $(i = 1, ..., 9)$ at $T = 0.02\epsilon$ we have confirmed that the initial orientation does not crucially affect the restitution coefficient.

5 The results of our numerical simulation

5.1 The relaxation of velocity autocorrelation function

At first, we have carried out the contact simulation for two identical nanoclusters contacting each other. From our simulation, we verify that the Hertzian contact theory can be used without introduction of any fitting parameters[15]. The details will be reported elsewhere. Another purpose of the contact simulation is to check whether eq.(12) can be used in our system. For this purpose, we make the two identical clusters contact each other under the mirror symmetric configuration, and equilibrate them at $T = 0.03\epsilon$. After the equilibration, we leave those clusters, and record the time evolution of the velocity of 14 atoms near the center of mass of the upper cluster, and collect 50 samples with different initial velocities for all the atoms, *i.e.* we average the data under 700 different samples to calculate VACF .

Figure 2 is the result of VACF near the center of mass of the upper cluster in our simulation. The upper envelope line is given by $f(x) = 0.0029x^{-1/2}$, which is consistent with the theoretical prediction.

5.2 The collision of two identical clusters

In this subsection, we show the results of out simulations for colliding two identical nanoclusters. We mainly simulate the two cases for the interaction between different clusters: the completely repulsive case with $a = 0.0$, and the weakly cohesive case with $a = 0.2$, where a is the cohesive parameter in eq. (17) between different clusters.

Let us show the sequential snapshots of two colliding clusters. Figure 3 (a) and (b) show the collisional behavior in the case of $a = 0.0$ and $a = 1.0$, respectively. It should be noted that we demonstrate the case of $a = 1.0$ to emphasize the difference between the noncohesive collision and the cohesive collision. In Fig. 3 (b), we can observe the elongation of clusters along the $z-$axis before the separation, while we do not observe any elongation of clusters before the separation in Fig. 3 (a). This elongation in Fig. 3 (b) is the result of the cohesive interaction between two clusters.

5.3 The relations between the restitution coefficient and the colliding speed

Here, we numerically investigate the relation between the restitution coefficient and the colliding speed. Figure 4 shows the relation between the restitution coefficient e and the relative speed of impact $V/\sqrt{\epsilon/m}$ in purely repulsive collisions with $a = 0$. The initial configurations of two colliding clusters are assumed to be mirror symmetric. The cross points and error bars in Fig.4 are, respectively, the average and the standard deviation of 100 samples for each colliding speed. From Fig. 4, we confirm that the restitution coefficient e decreases with the increase of the colliding speed $V/\sqrt{\epsilon/m}$. When the colliding speed is $V = 0.02\sqrt{\epsilon/m}$ at $T = 0.02\epsilon$, the average of e becomes 1.04 which is slightly larger than unity. It is interesting that our result can be fitted by the quasi-static theory of low-speed impacts $1 - e \propto V^{1/5}$[5, 6, 7] when the restitution coefficient in the limit $V \to 0$ is replaced by a
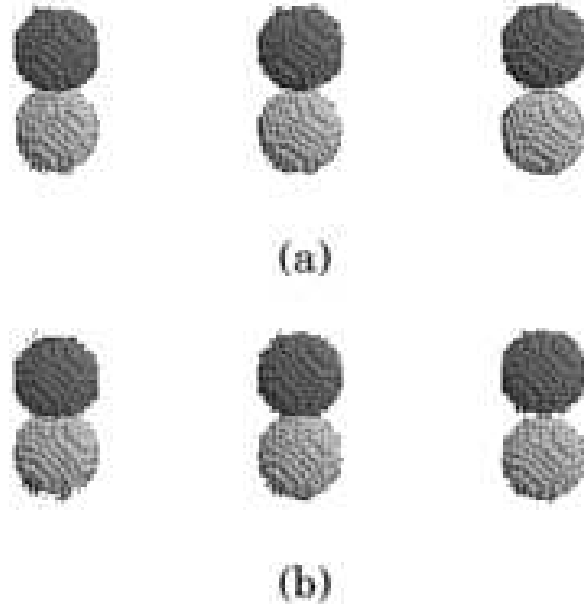
Figure 3: Sequential snapshots of two colliding clusters in the cases of (a) a=0.0 and (b) a=1.0.

constant larger than unity. Indeed, the solid and the broken lines in Fig. 4 are fitting curves of $e = \alpha_1 - \alpha_2 \left(V/\sqrt{\epsilon/m}\right)^{1/5}$, where α_1 and α_2 depend on material constants of colliding bodies and T.

We also briefly discuss the effect of the size dependence on the result. The results of our simulation for $N = 433$, which is a 11 layered spherical cut of FCC lattice, cannot be approximated by the quasi-static theory, where the restitution coefficient seems to be almost independent of the colliding speed in the wide range of the impact speed. On the other hand, we cannot find any systematic relation between the restitution coefficient and the colliding speed in the simulation for $N = 1466$ which is a 17 layered spherical cut of FCC lattice. This can be attributed to the melting on the surface of the cluster. The details of the melting properties will be reported elsewhere.

Next, we investigate the weakly cohesive collisions with $a = 0.2$ between those two clusters. Figure 5 shows the relation between restitution coefficient and impact speed, where 100 samples are taken for each colliding speed at the initial temperature $T = 0.02\epsilon$. When there is the cohesive interaction between two colliding clusters, the relation has a peak as suggested by Brilliantov *et al.*[9]. In the figure, the open circles are the numerical results obtained by solving the equation developed by Brilliantov *et al.*[9]. To solve this equation, we evaluate the values $\gamma \simeq 0.026\sqrt{\epsilon m/\sigma}$ from the calculation of the attractive interaction between two clusters.[1] The theoretical result in Fig. 5 suggests that the restitution coefficient is insensitive to the colliding speed

---

[1]The surface tension γ can be calculated from the attractive potential. The method of our evaluation will be reported elsewhere.
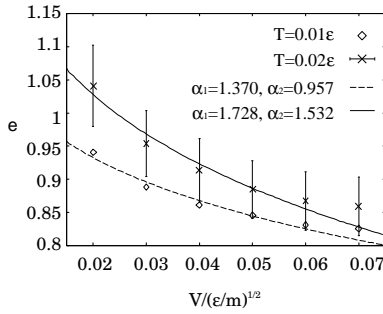
Figure 4: The relation between colliding speed and restitution coefficient in the case of $a = 0.0$ at $T = 0.01\epsilon$ and $T = 0.02\epsilon$.
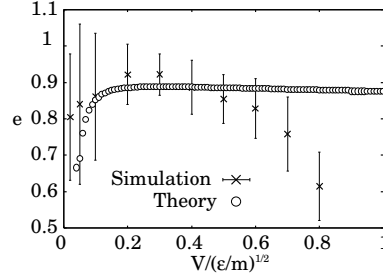

Figure 5: The relation between colliding speed and restitution coefficient in the case of $a = 0.2$. One cluster consists of 682 atoms. The cross points and open circles are, respectively, the result of our simulation and the theory in ref.[9].

for the large colliding speed, though the restitution coefficient slightly decreases with the increment of the colliding speed.

5.4 The frequency distribution functions of the restitution coefficient

Here, we show our numerical results on the frequency distribution function of the restitution coefficient, which strongly depends on the cohesive parameter. Figure 6 shows histograms of the restitution coefficients for both the purely repulsive collisions and the cohesive collisions $a = 0.2$. When there is no cohesive interaction between the two clusters, the frequency distribution function is roughly represented by the Gaussian distribution function. On the other hand, the frequency distribution function is irregular when the cohesion exists. It is notable that the anomalous events for e to exceed the unity becomes rare when there is the attractive interaction between clusters, though a few percent of the collisions still exhibit the anomalous impacts. This is because two clusters are coalesced with each other in the slow impacts. Therefore, the frequency distribution function for $a = 0.2$ has a steep peak near $e = 1$.

In Fig.6(b), there are the first and the second peaks around $e = 0.4$ and $e = 0.65$, respectively. The collisional modes observed around these peaks are the rotational bounces after the collisions, while the most of bounces are not associated with rotations in the vicinity of the third peak around $e = 1$. It is reasonable that the excitation of macroscopic rotation lowers the translational energy to decrease the restitution coefficient.

For cohesive collisions, we can categorize the rebound behaviors of the colliding clusters into four patterns (see Fig. 7): (a) $n = 0$ (complete adhesion), (b) $n > 1$, (c) $n = 1$ and $e < 1$, and (d) $n = 1$ and $e > 1$, where n is the number of collisions in each impact process. The collision with $n > 1$ can take place, when the attractive interaction between the colliding clusters exists. Indeed, if the rebound speed is not
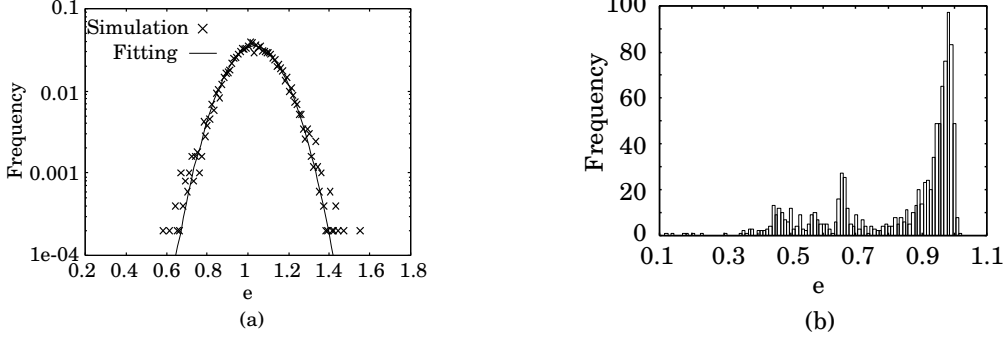
9

(a)

(b)

Figure 6: Histograms of the restitution coefficients for (a) $a = 0.0$, $V = 0.02\sqrt{\epsilon/m}$, and (b) $a = 0.2$, $V = 0.1\sqrt{\epsilon/m}$. The guide line in the left figure is the Gaussian fitting of the data.

large enough, the rebounded clusters are attracted to have the second collision. We call the case with $e > 1$ and $n = 1$ the anomalous impact, but there are some other characteristic collisions as can be seen in Fig. 7.

Similarly, we categorize the collisions into four groups as a function of the cohesive parameter under the fixing colliding speed $V = 0.02\sqrt{\epsilon/m}$ (Fig. 8). It is obvious that there are two categories, (c) and (d), in noncohesive collisions, while the probability to occur (a) or (b) increases as a increases. It is interesting that Fig.8 is almost the mirror symmetric one of Fig. 7. This fact suggests that the cohesive parameter plays a role of the impact speed. The relation between the impact speed and the cohesive parameter will be discussed elsewhere.
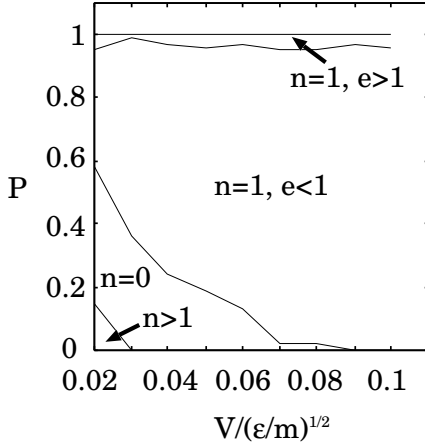

Figure 7: Probabilities classified by collision modes observed in cohesive collision with $a = 0.2$.
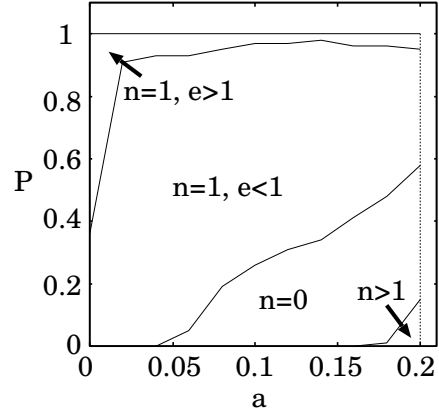

Figure 8: The probability classified by four modes at $V = 0.02\sqrt{\epsilon/m}$.

10

6 Discussion and conclusion

In this paper, we study collisions of nanoclusters which are thermally activated. We also discuss the effects of cohesive force between the colliding two clusters. Although the results are preliminary, we believe that our paper includes some potentially important results for the nanoscience. Let us briefly discuss our results. An anomalous impact with $e > 1$ occurs with a finite probability even for realistic situations (see Fig. 8). This is an important indication, though the cohesive force between the colliding clusters suppresses such events in the low speed collisions. We also find an interesting similarity in the roles of the impact speed and the cohesive parameter (Fig. 8). It is more interesting that the cluster is fluidized when the cluster is large. There is capillary instability at the surface of the large cluster, because the influence of the attractive binding force from the center of mass is weaker, the size of the cluster is larger. The quantitative discussion will be discussed elsewhere.

In conclusion, we study the impact of thermally activated nanoclusters numerically. We confirm that VACF satisfies $\phi(t) \sim 1/\sqrt{t}$. The restitution coefficient seems to be consistent with the quasi-static theory when there is no attractive interaction between the two colliding clusters, while the restitution coefficient has a peak at a finite value of the impact speed, when the attractive interaction exists. The anomalous impacts which have $e > 1$ commonly take place in purely repulsive collisions, while such an impacts become rare in cohesive collisions. The frequency distribution function satisfies Gaussian for purely repulsive collisions and has some peaks in cohesive collisions.

Acknowledgements

References

[1] C. Maes and H. Tasaki: Lett. Math. Phys. **79**, 251(2007).

[2] H. Tasaki: J. Stat. Phys. **123**, 1361 (2006).

[3] M. Y. Louge and M. E. Adams: Phys. Rev. E **65**, 021303 (2002).

[4] H. Kuninaka and H. Hayakawa: Phys. Rev. Lett. **93**, 154301 (2004).

[5] G. Kuwabara and K. Kono: Jpn. J. Appl. Phys. **26**, 1230 (1987).

[6] N. Brilliantov, F. Spahn, J.-M. Hertzsch, and T. Pöschel: Phys. Rev. E, **53**, 5382 (1996).

[7] W. A. Morgado and I. Oppenheim: Phys. Rev. E **55**, 1940 (1997).

[8] A. Awasthi, S. C. Hendy, P. Zoontjens, S. A. Brown, and F. Natali: Phys. Rev. B, **76**, 115437 (2007).

[9] N. V. Brilliantov, N. Albers, F. Spahn, and T. Pöschel: Phys. Rev. E **76**, 051302 (2007).

[10] M. Kalweit and D. Drikakis: J. Compt. Theor. Nanoscience **1**, 367 (2004).

[11] L. J. Lewis, P. Jensen, and J-L Barrat: Phys. Rev. B, **56**, 2248(1997).

[12] O. Knospe, A. V. Glotov, G. Seifert, and R. Schmidt: J. Phys. B: At. Mol. Opt. Phys. **29**, 5163(1996).

[13] Y. Yamaguchi and J. Gspann: Phys. Rev. B, **66**, 155408(2002).

[14] A. Tomsic, H. Schröder and K. -L. Kompa and C. R. Gebhardt: J. Chem. Phys. **119**, 6314 (2003).

[15] H. Kuninaka and H. Hayakawa, arXiv:0707.0533v1.

[16] R. Zwanzig, Nonequilibrium Statistical Mechanics (Oxford University Press, 2001).

[17] R. Kubo, M. Toda and N. Hashitsume, Statistical Physics II :Nonequilibrium Statistical Mechanics (Springer-Verlag, 1992).

[18] M. Rieth: *Nano-Engineering in Science and Technology* (World Scientific, 2003).

[19] J. M. Haile and S. Gupta: J. Chem. Phys. **79**, 3067 (1983).

[20] H. C. Andersen: J. Chem. Phys. **72**, 2384 (1980).

Hisao Hayakawa, Yukawa Institute for Theoretical Physics, Kyoto University, Kitashirakawa-oiwakecho, Sakyo-ku, Kyoto 606-8502, Japan

Hiroto Kuninaka, Department of Physics, Chuo University, Bunkyo-ku, Tokyo 112-8551, Japan